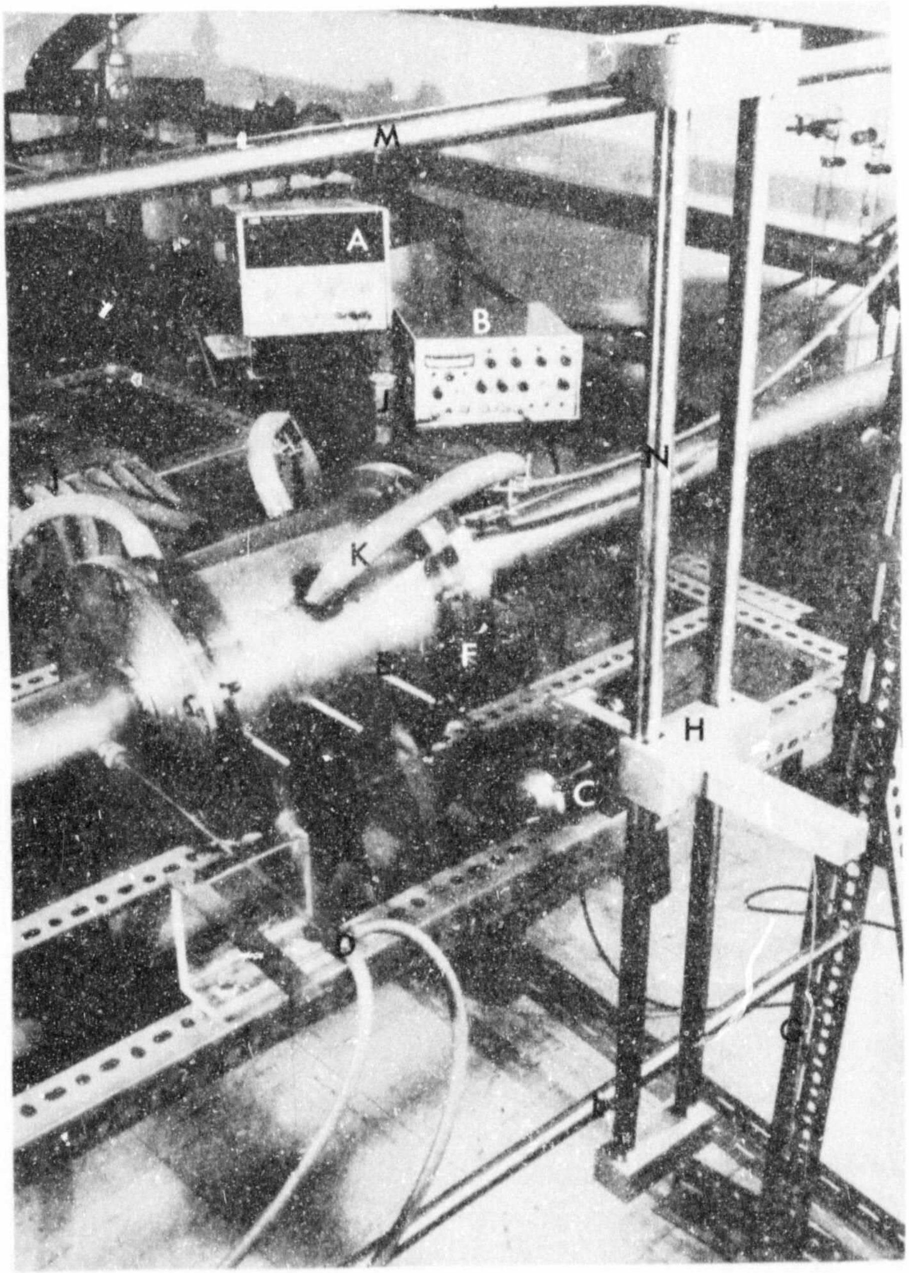

KEY

A. Digital voltmeter
B. Anemometer
C. Traversing dial
D. Pitot tube
E. Wooden plug
F. Hot-wire support
G. Handy angle support
H. Slider
I. Manifold
J. Damping capacitor
K. Rubber tubing
L. Adjusting screw
M. Horizontal runner
N. Vertical runner

Fig 5.6 - The test rig

5.5 Hot-Wire Anemometry and Traversing Mechanism

A Disa type 55D01 constant temperature anemometer unit was used for the measurements of the axial and radial velocities within the porous pipe, using as transducers four hot-wire probes Disa type 55P11. These hot-wire probes, of the miniature variety, were mounted on Disa type 55H21 probe holders, of 4 mm outside diameter, which were 225 mm long and thus able to traverse the distance through the probe guides to the far side of the test specimen.

The output from the anemometer unit was fed into a Hewlett Packard digital voltmeter via a capacitor and resistance connected in parallel. These components were used to damp any small fluctuations in the velocities and allowed direct mean velocity readings from the voltmeter.

The traversing mechanism, also made by Disa (type 55H01), was used to position the probes at various locations across the porous pipe. For slipless traversing a pinion drive shaft was used which meshed with a toothed probe support, containing the probe holder and probe (see Fig 5.5). The mechanism was driven by a manually operated drive unit. The traversing range was 100 mm i e 10 mm per revolution of the dial.

To ensure that the velocity readings were not effected significantly from leakage through the probe guides, a rubber seal was placed around the probe holder and this enabled the clearance between the guide and holder to be sealed. While not in use the probe guides were sealed with wooden plugs (see Fig 5.5).

Measurements of the air temperature, as indicated by thermocouples 2 and 3 were made at frequent intervals, as hot-wire probes are extremely sensitive to temperature variations. The readings on the voltmeter had to be corrected according to the air temperature. Full details are given in the appendix.

The traversing mechanism was supported by the framework shown in Fig 5.6. This was designed to provide ease of movement along the pipe, when changing from one probe guide to the next, by simply sliding the traversing mechanism along on the tubular runners. It was rigidly supported to prevent undue vibrations from damaging the hot-wires. An adjustment screw at the lower end allowed for inclination of the traversing mechanism. The height could be varied by sliding it along the vertical runners.

To measure both axial and radial components of velocity, traverses had to be made with the probe wire parallel to the air stream and then perpendicular to it. The reasons for this are explained in Chapter 6. Readings from the voltmeter in volts enabled the velocities to be determined according to calibration curves. The details of the calibration of the hot wires is given in the appendix.

5.6 The experimental Procedure

With the by-pass gate valve in the fully open position the blower was switched on. The speed was adjusted by means of the variable speed drive, to give the maximum flow rate required through the apparatus for a series of tests. The cooling water for the annular cooler was then turned on.

The by-pass gate valve was gradually closed to a convenient position thus allowing a certain proportion of the air available from the blower to pass through the working section. Tests were then run for various positions of the outlet valve which was used to force more and more air through the walls of the porous specimen into the manifold. As the oulet valve was closed, not only did more air flow through the walls of the porous specimen, but also through the by-pass which could have been closed more in order to maintain the same initial flow rate through the apparatus. This was not done, however, because it was not thought necessary to conduct all the tests at a given flow rate as the results were analysed in terms of non dimensional parameters which are described in Chapter 6.

At this stage some tests were conducted with no air extracted through the walls. This was achieved by screwing closed clips which were located on each length of rubber hosing connecting the working section to the manifold. This forced all the air to pass through the outlet valve.

Before any readings were taken the blower was left running with the valves in the test positions until the temperature of the air, as indicated by the thermocouple outputs, had ceased to rise. This usually took about thirty minutes to an hour depending on the loading on the blower and the weather conditions. This time interval also allowed the entire working section to reach an equilibrium temperature. The test specimen was isolated from the atmosphere by two layers of insulating air and thus was able to achieve and maintain the same temperature as the air in the porous pipe. This temperature did not vary throughout the entire test pipe as shown by a thermocouple traverse.

The atmospheric pressure was read in milli-meters of mercury from a Fortin barometer and the reading was corrected to account for the atmospheric temperature.

The potentiometer was adjusted for each thermocouple and readings of the output were taken in milli-volts, which were converted via the thermocouple calibration charts to give the air temperature.

The next observations to be made were the orifice plate readings. To calculate the volume flow rate through an orifice plate according to British Standards BS 1042 values were required for the following:

(i) $m = \frac{d^2}{D^2} = \frac{(\text{orifice diameter})^2}{(\text{pipe inside diameter})^2}$

(ii) Static pressure at the high pressure side

(iii) Pressure difference across the orifice plate

(iv) Temperature at the high pressure side.

The orifice and pipe diameters were measured before the testing commenced with vernier calipers an average of three readings being taken for each. The static pressures at the high pressure sides were calculated from the gauge pressures indicated by the mercury manometers added to the atmospheric pressure. The pressure differences were read directly from U-tube manometers as described in section 5.3. The temperatures were already available.

From these four readings the volume and mass flow rates of the air were calculated by means of the formulae given in Chapter 6. The difference between the flow rate indicated by orifice plate 1 and plate 2 gave a direct value for the amount of air being expelled through the porous specimen.

Next a velocity traverse was made at the entrance to the working section using the miniature pitot tube. Readings of the dynamic pressure were taken at 25 millimeter intervals across the pipe. The static pressure was also measured at this location. The velocity profile was calculated from the dynamic pressure observations and the values were fed into a computer programme which numerically evaluated the volume and mass flow rates through the pipe by integrating the velocity profile. Details of this technique are given in the appendix.

Readings of static pressure were taken at positions 3, 4, 5, 6 and 7. The temperature of the air was monitored again and any change was noted.

Hot-wire probe number one was placed in its holder and positioned in the support attached to the traversing mechanism. The decade resistance settings on the anemometer unit were adjusted to the value obtained during the calibration of probe number one. The anemometer was switched to internal thus heating the hot-wire. The traversing mechanism was positioned at the entrance to probe guide number one. The position of the probe was varied until the wire was perpendicular to the axis of the pipe. The holding mechanism was tightened. The dial attached to the driving unit of the traversing rig was turned until the hot-wire reached a position at the entrance to the porous specimen. The first reading of voltage on the digital voltmeter was taken at this position. Due to the damping effects of the capacitor connected to its input the voltmeter took a few minutes to attain its final reading. The probe was then advanced fifty millimeters and another reading taken. The procedure was repeated across the entire test specimen. Every time the probe was moved it was necessary to ensure that the rubber seal was firmly in place on the end of the probe guide. The probe was returned to approximately the centre of the pipe and was turned through ninety degrees, so that now the probe wire was parallel to the axis of the pipe. This was done near the centre of the pipe to avoid contact with the pipe wall and possible breakage of the hot-wire. The probe was then returned to its initial position, on the near side of the specimen and the traversing procedure repeated. During these measurements the probe guides two, three and four were sealed with the wooden plugs.

This series of readings were repeated for probes two, three and four.

It was important that the temperature of the air was examined frequently, since the hot-wire readings had to be corrected for temperature variations. (See Appendix).

Whole series of tests were run with the blower set at different speeds giving a range of volume flow rates from 510 to 1 020 m^3/hr.

CHAPTER 6

PRESENTATION AND DISCUSSION OF RESULTS

6.1 Introduction

This chapter is divided into three sections. The first (section 6.2) presents results obtained from the computer programme. The reduction of the theoretical data is discussed with reference to various non-dimensional parameters and the scope and limitation of the theoretical solutions are examined.

The second section (section 6.3) contains a discussion of the experimental results and their expected limits of accuracy. The methods of data reduction are explained in detail, and reasons for using certain non-dimensional parameters are given.

The third and final section (section 6.4) compares and contrasts the results of sections 6.2 and 6.3 with those of other authors, discussed in Chapter 2. Comparisons are made by means of graphs where possible.

6.2 The Theoretical Results

The principal results from the computer programme are tabulated in the appendix. Many more results were obtained but it was decided that only the important ones would be listed.

The bulk of the theoretical results were obtained for flat inlet and outlet velocity profiles through the pipe as these were thought to be close approximations to fully developed turbulent pipe flow profiles. The no-slip condition at the wall was not simulated. The porous pipe was preceded and followed by lengths of non porous piping (see section 3.9) to enable a realistic model to be studied. The length to diameter ratio of the porous pipe was 5,0 and the overall length to diameter ratio of the whole model was 10,0.

It was described in section 3.7 how the programme calculates a pressure coefficient, Cp, at positions inside the pipe and on the pipe surface. This pressure coefficient relates the change in pressure along the pipe to the pressure on the pipe axis at the inlet. Thus suction through the porous surface will be characterised by a rise in the pressure coefficient and blowing by a decrease.

For ideal flow (i e potential flow) there are no pressure losses along the pipe due to skin friction and so, in the suction case, pressure recovery is directly related to the decrease in velocity. The maximum value of the pressure coefficient is thus + 1,0. This is achieved when all the fluid entering the pipe is extracted through the porous wall, and there is no axial outflow.

Figure (6.1) shows the variation of Cp with axial distance along the pipe model, for various radial positions. The porous section is indicated by vertical dark lines. The axial distance has been non dimensionalised with respect to the diameter of the pipe, this choice is purely arbitrary and another parameter ($L/4\beta$) based on the suction coefficient will be discussed later. The radius of the pipe during the calculations was unity and so the radial positions, indicated by r, may be thought of as being non-dimensionalised with respect to the radius of the pipe.

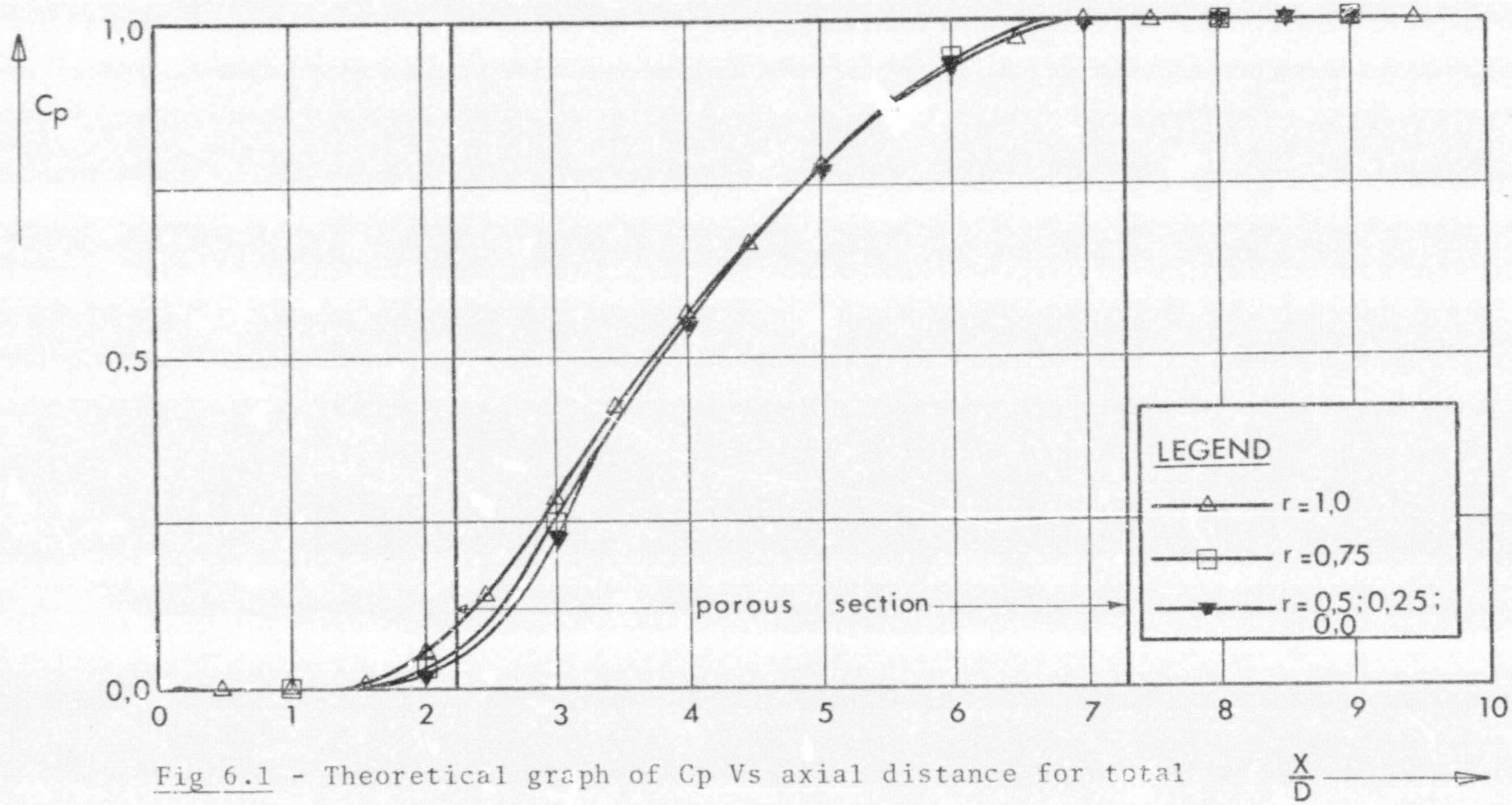

Fig 6.1 - Theoretical graph of Cp Vs axial distance for total mass extraction

From figure 6.1 it can be seen that there is virtually no pressure gradient in the radial direction as some of the curves coincide while others very nearly do, for a fixed axial position. The largest differences and hence pressure gradients are experienced at the entrance to the porous section in the proximity of the pipe wall. This is to be expected as the boundary conditions at the pipe wall suddenly become discontinuous here and the flow has to adapt to the change. At the exit, although the boundary conditions are again discontinuous, the flow has almost been reduced to zero and so these effects are not as strong.

So far the discussions have involved only flows where all the fluid is extracted through the walls. The programme was run for a variety of extraction rates through the wall. It is necessary to define a fluid transfer coefficient so that the results for the various flow situations may be compared. The coefficient, β, is defined as follows:

$$\beta = \frac{V_r}{V_k} \quad . \quad . \quad . \quad . \quad . \quad . \quad . \quad . \quad . \qquad (6.1)$$

Thus for the tests done with constant mass transfer along walls β will be constant. V_r is positive for outflow and negative for inflow, this means that for suction β will be positive and for blowing negative. For a porous pipe of given dimensions and for β increasing positively more and more fluid will be extracted through the walls.

Figure 6.2 shows a comparison of pressure recoveries for various values of β. The curves are similarly shaped and the limit of recovery is shown by the total extraction case. An interesting feature to note is that the higher the suction rates the more convex the curves become. At the low values of β the curves are definitely concave.

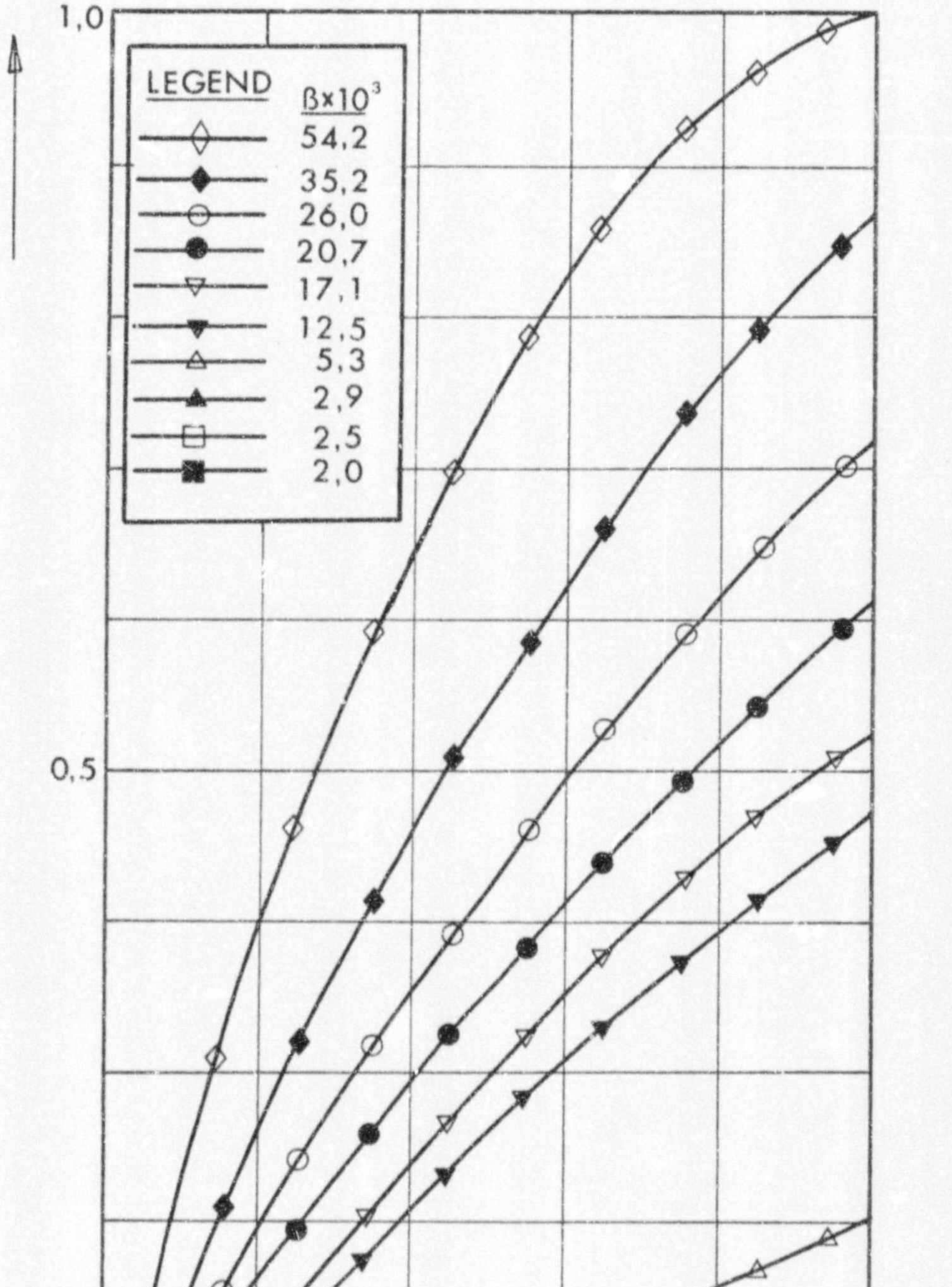

Fig 6.2 - Theoretical variations of Cp for different values of β (positive)

The values of pressure coefficient were evaluated on the surface of the pipe, but it has already been mentioned that these closely resemble the pressures on the axis (see figure 6.1). The shapes of the curves are discussed in more detail later in the section.

Figure 6.3 illustrates the same principles as figure 6.1 but for the blowing case. For this flow situation ideally, there is no limit on the negative value of pressure coefficient obtained. As more fluid is introduced through the walls of the pipe so the axial velocity in the pipe increases and the pressure drops. The limit in the practical case would be reached when the resulting flow became choked. The same features are apparent on these curves, as in figure 6.1. The radial pressure gradients are small, except in the vicinity of the porous pipe ends as shown by change in pressure with radial distance for a given axial position. The pressure gradients can be seen to be more noticeable in the regions of higher velocities which for the blowing case are obviously at the exit of the pipe. The pressure decrease along the surface of the porous pipe due to various blowing rates is illustrated in figure 6.4, again the curves are similarly shaped, and they all appear to be convex.

Figures 6.2 and 6.4 both show families of curves, similarly shaped, for various values of β, positive and negative. In the form that they are drawn it is difficult to compare them further other than saying they are 'similar'. The difficulty arises because, for a pipe of given geometry, different values of β cause there to be different proportions of flow to be added or extracted through the surface. It would seem more logical to compare results from tests all with say, total mass extraction, or at least the same proportion of extraction. This means that for different values of transfer coefficient β, the pipe's

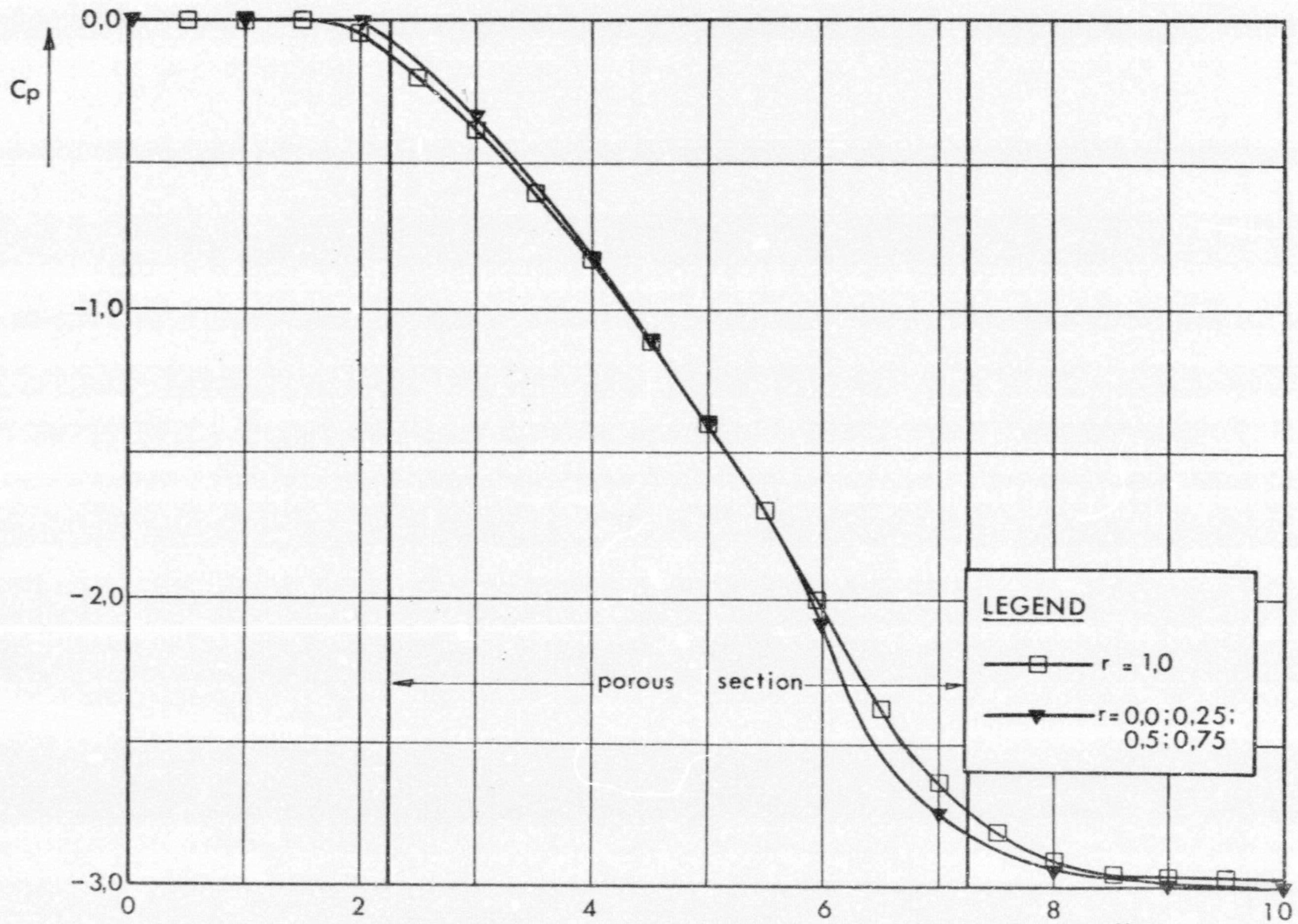

Fig 6.3 - Theoretical graph of Cp Vs axial distance for mass addition.

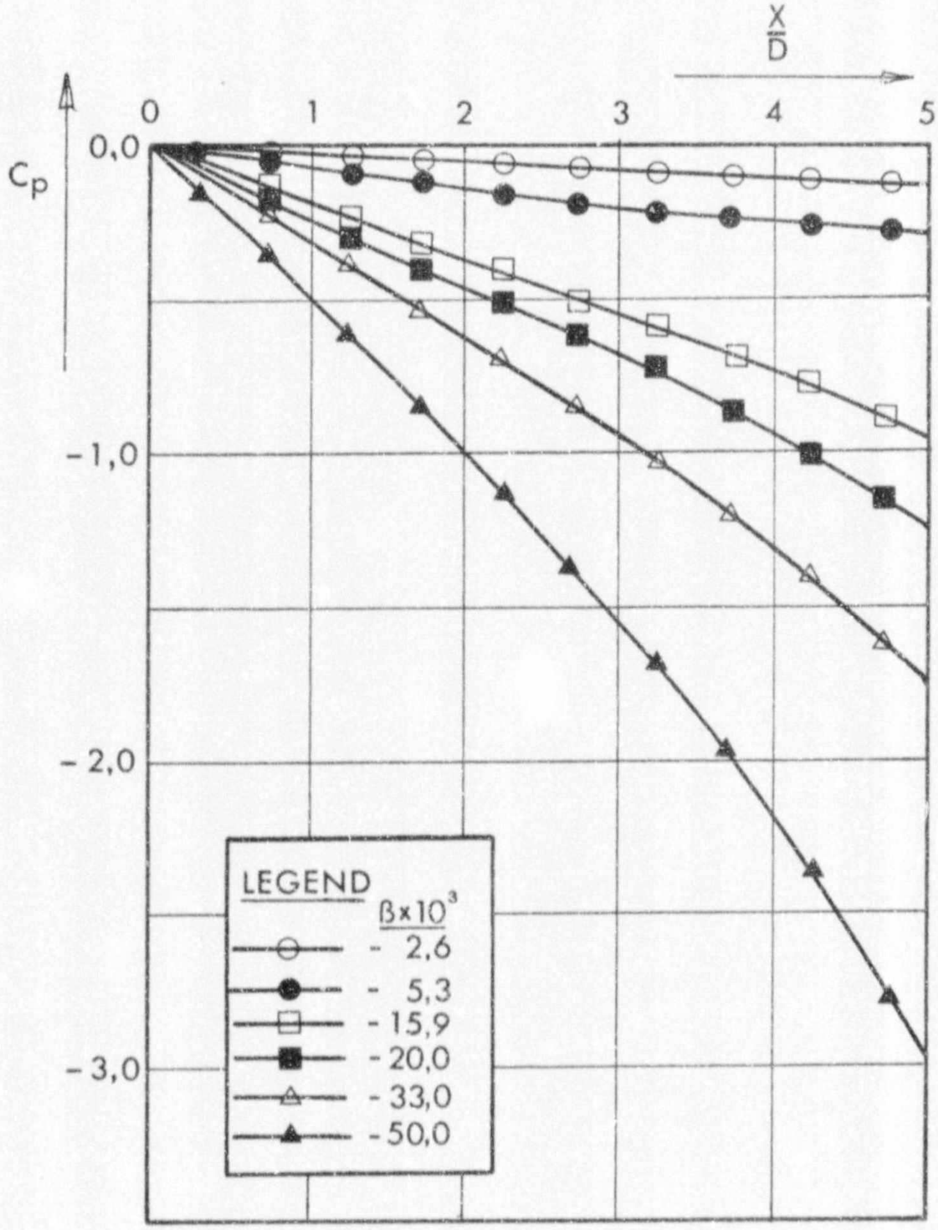

Fig 6.4 - Theoretical variations of Cp for different values of β (negative)

geometry would have to change for the same proportion of extraction to be achieved.

For the suction tests it is natural to choose total extraction as the limit and calculate, for various values of β, how the pipe geometry has to be changed in order to achieve total extraction. In essence it means that instead of non-dimensionalising the axial distance with respect to the actual diameter of the porous pipe it is non-dimensionalised with respect to a ficticious length L_f which is calculated as follows:

Volume flow rate at inlet to pipe $= \frac{\pi D^2}{4} V_k$ . . . . (6.2)

Volume flow rate through the wall $= \pi D V_r$ per unit length . (6.3)

If L_f is the length of pipe required for total extraction then:

$$L_f = \frac{DV_k}{4V_r} = \frac{D}{4\beta} \quad \ldots \ldots \ldots \quad (6.4)$$

When figure 6.2 is replotted non-dimensionalising the axial distance with respect to L_f the curves collapse onto one as illustrated in figure 6.5. At first it seems strange that the concave ones should co-incide with the convex, but it becomes apparent on closer inspection that at low values of Cp all the convex curves are in fact slightly concave, and this is the region onto which the concave curves are collapsing.

The same may be done for the blowing curves of figure 6.4. The non-dimensionalising length was chosen in a similar way to before. This time the length L_f was defined as that length required such that the total mass addition

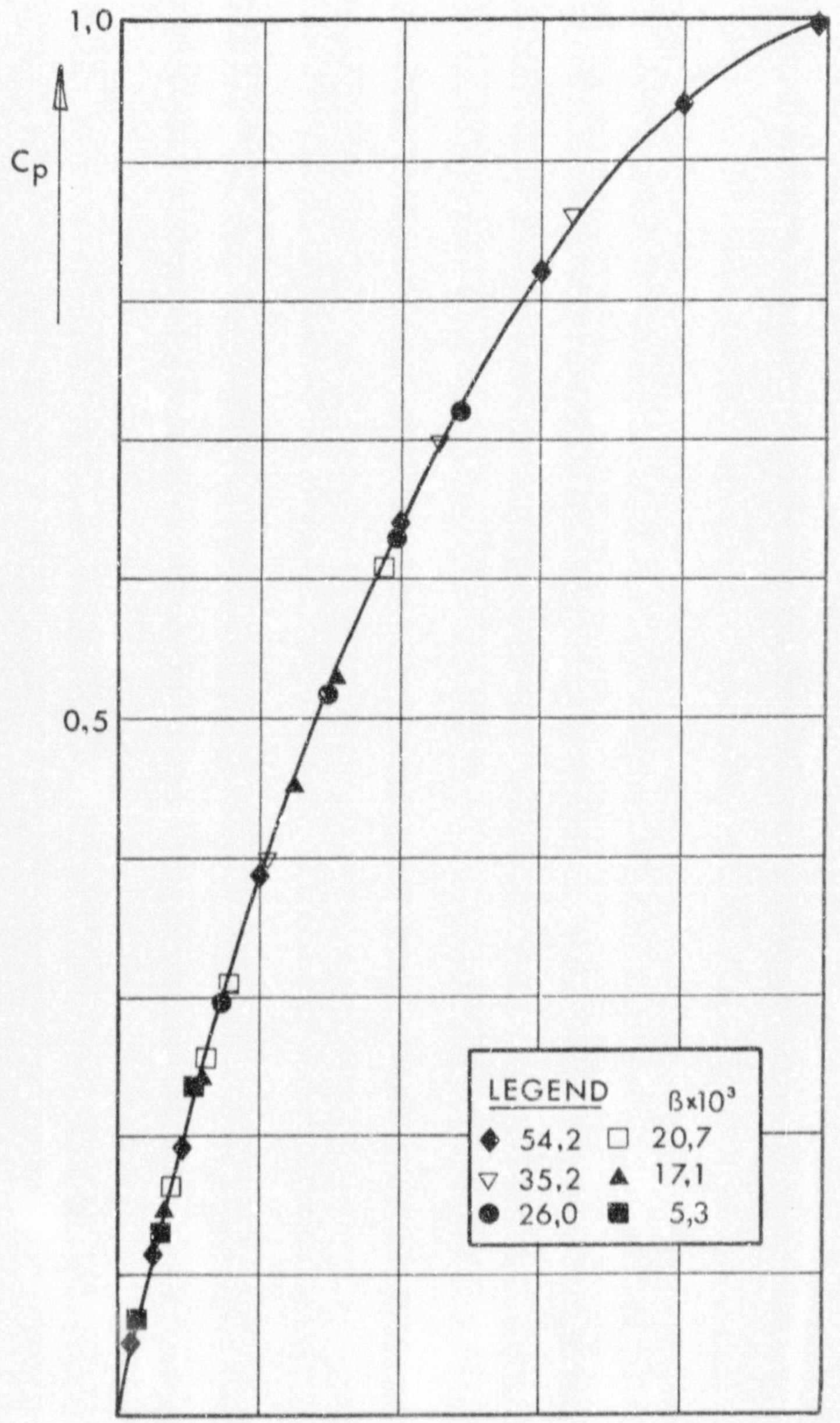

Fig 6.5 - Non-dimensionalised pressure curves for mass extraction

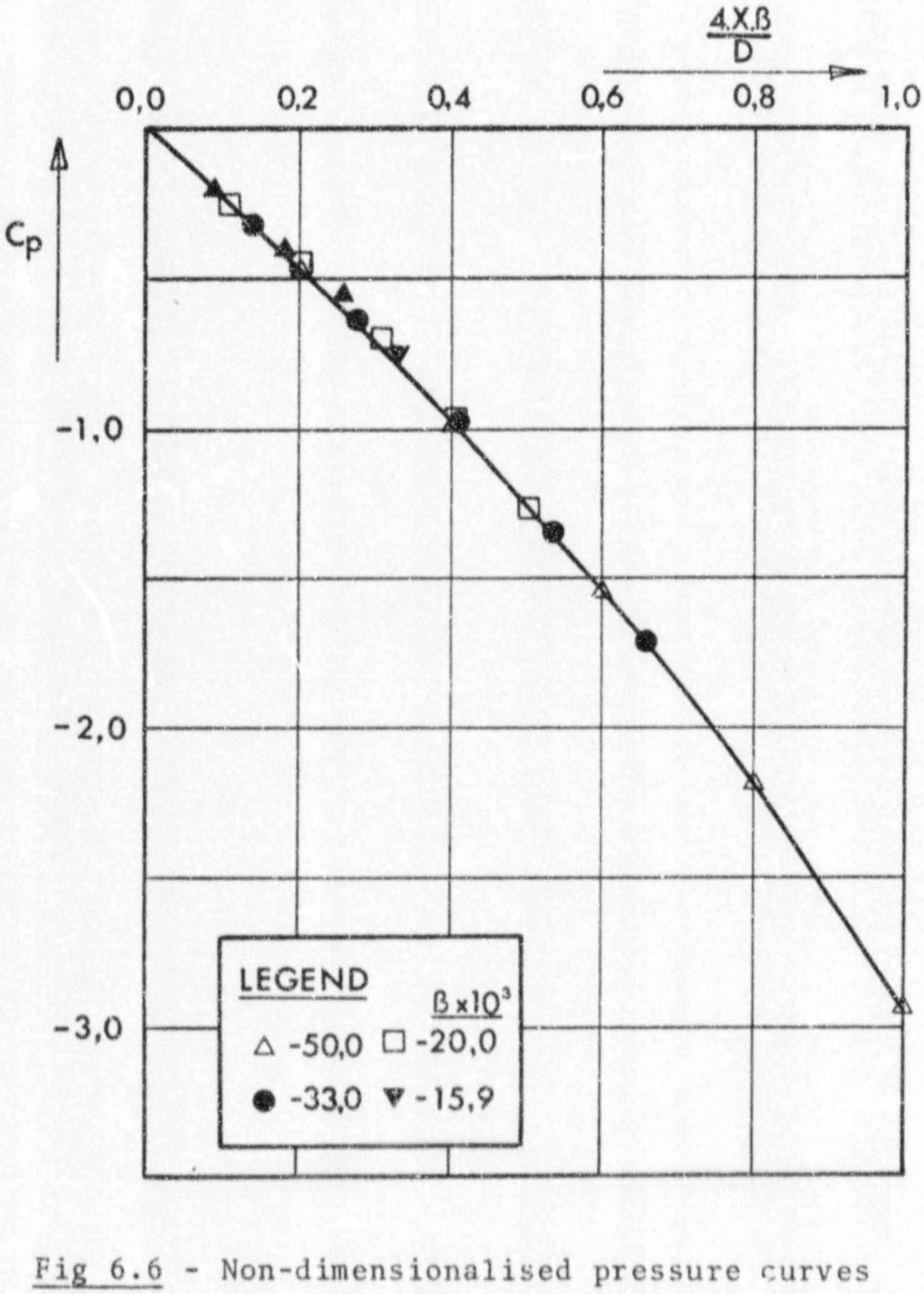

Fig 6.6 - Non-dimensionalised pressure curves for mass addition

was equal to the initial axial inflow. This means that the outflow at the exit to the pipe is double that at the inlet. Figure 6.6 shows the result of non-dimensionalising figure 6.4 in this way. Again all the curves collapse onto one curve.

The mass transfer coefficient, as it has been used so far, was defined at the entrance to the pipe. It will be interesting to see how the local mass transfer coefficient varies along the pipe. A coefficient may be evaluated at positions along the pipe. If β_o is now referred to as the coefficient evaluated at the inlet to the pipe then:

$$\beta_o = \frac{V_r}{V_k} \quad . \quad . \quad . \quad . \quad . \quad . \quad . \quad . \quad . \qquad (6.5)$$

and

$$\beta = \frac{V_r}{V_{max}} \quad . \quad . \quad . \quad . \quad . \quad . \quad . \quad . \quad . \qquad (6.6)$$

Figure 6.7 shows values of β plotted aginst axial distance for various initial values of β_o. They are seen to increase from their value β_o, at the inlet to various values at the outlet depending on the proportions of fluid extracted. The upper curve is for total extraction. β tends to infinity at the end of the pipe because of vanishing axial velocity. When the curves are non dimensionalised with respect to L_f the curves take on a more regular form as shown in figure 6.8. They cannot obviously fall on one line as they are all plotted for different initial values of suction rates β_o, however they do all appear to be of a similar form. The upper curve in figure 6.8 gives values of the suction coefficient for the limiting case of total mass extraction. The curve asymptotes to $4x\beta_o/D$ equal to 1,0 and the asymptotic nature of the other

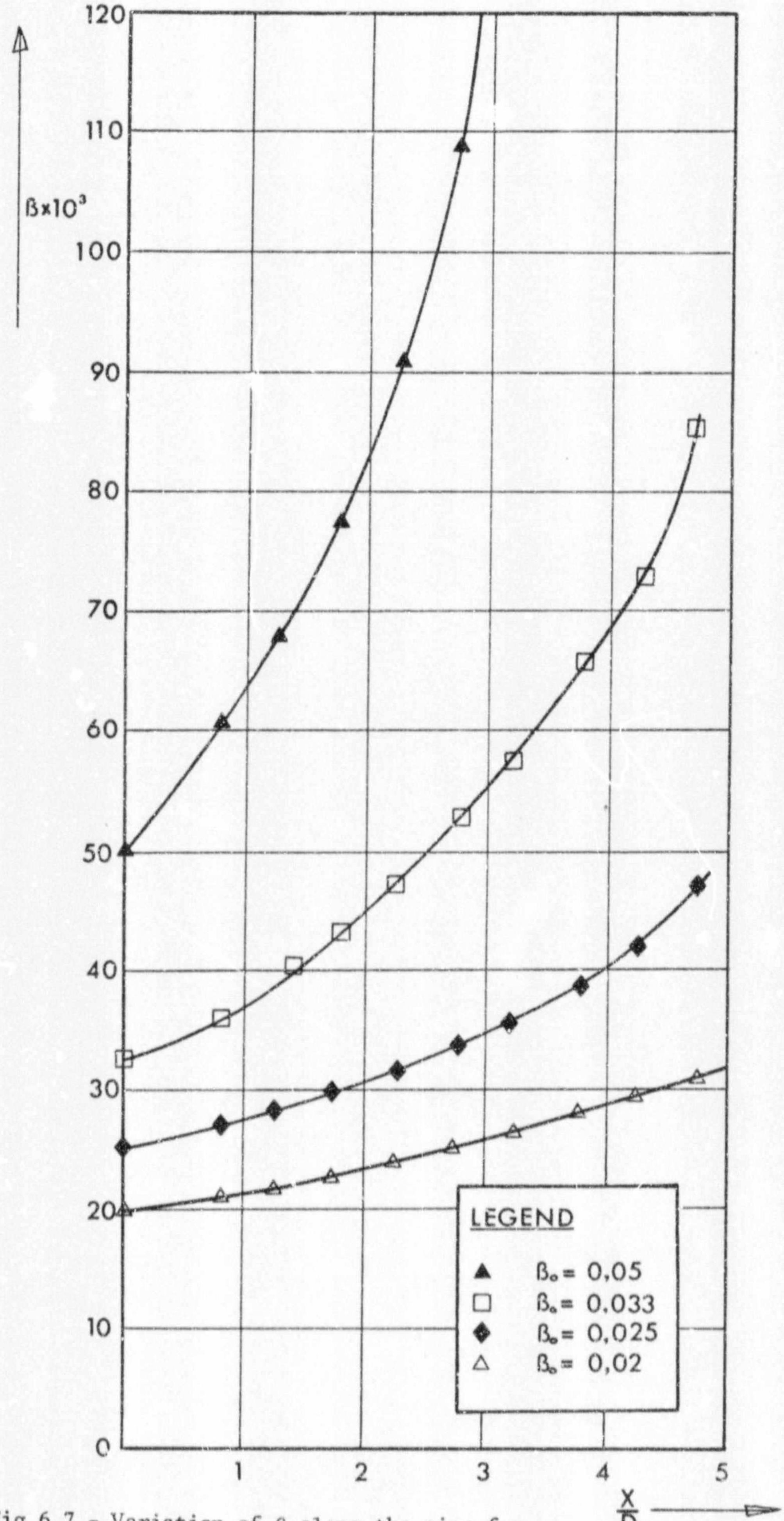

Fig 6.7 - Variation of β along the pipe for different initial suction rates

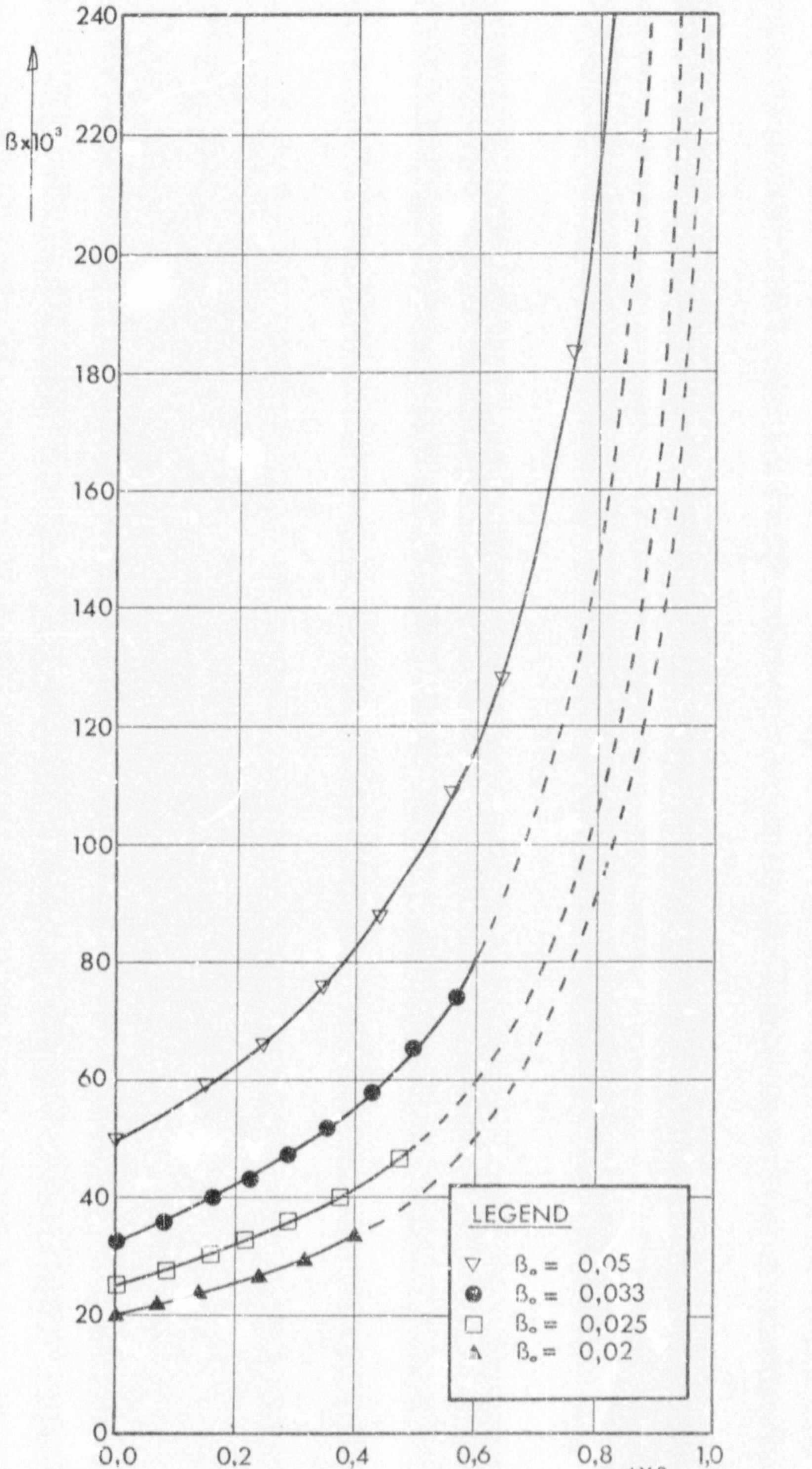

Fig 6.8 - Non-dimensionalised variation of β along the pipe for suction

curves has been shown by dotted lines. Thus it can be seen why the curves cannot be considered as parallel, since they all begin at different values and end at the same one.

Figures 6.9 and 6.10 show the same results for the blowing cases, indicated by negative values of the mass transfer coefficient. Figure 6.10 shows the curves of figure 6.9 non-dimensionalised. Although the curves of figure 6.10 are of a similar form they cannot definitely be said to asymptote to the same value, if any at all. The limit is probably $\beta = 0,0$, this indicates that the axial velocity has become infinite due to the unlimited addition of fluid. The curves simply show a decreasing (in magnitude) mass transfer coefficient with axial distance.

Figure 6.11 illustrates the effect of having a parabolic inlet velocity profile on the suction coefficient. The variation of suction coefficient along the pipe does not appear to be any different from the variations obtained with the flat profiles.

Figures 6.12 a) and b) were obtained from the contour plotting programme. The slight waviness that is introduced along several of the streamlines is a limitation of the plotting routine and not the input data. These plots are useful in examining the shape of the streamlines with a view to detecting irregular features such as crowding. In both figures 6.12 a) and b) there can be seen to be crowding of the streamlines in the vicinity of the entrance to the porous pipe, especially close to the pipe wall. This indicates that the potential is rapidly changing in this area and special attention must be paid to these regions during the analysis. It was already noticed from figure 6.1 that in this region the radial pressure gradients were highest.

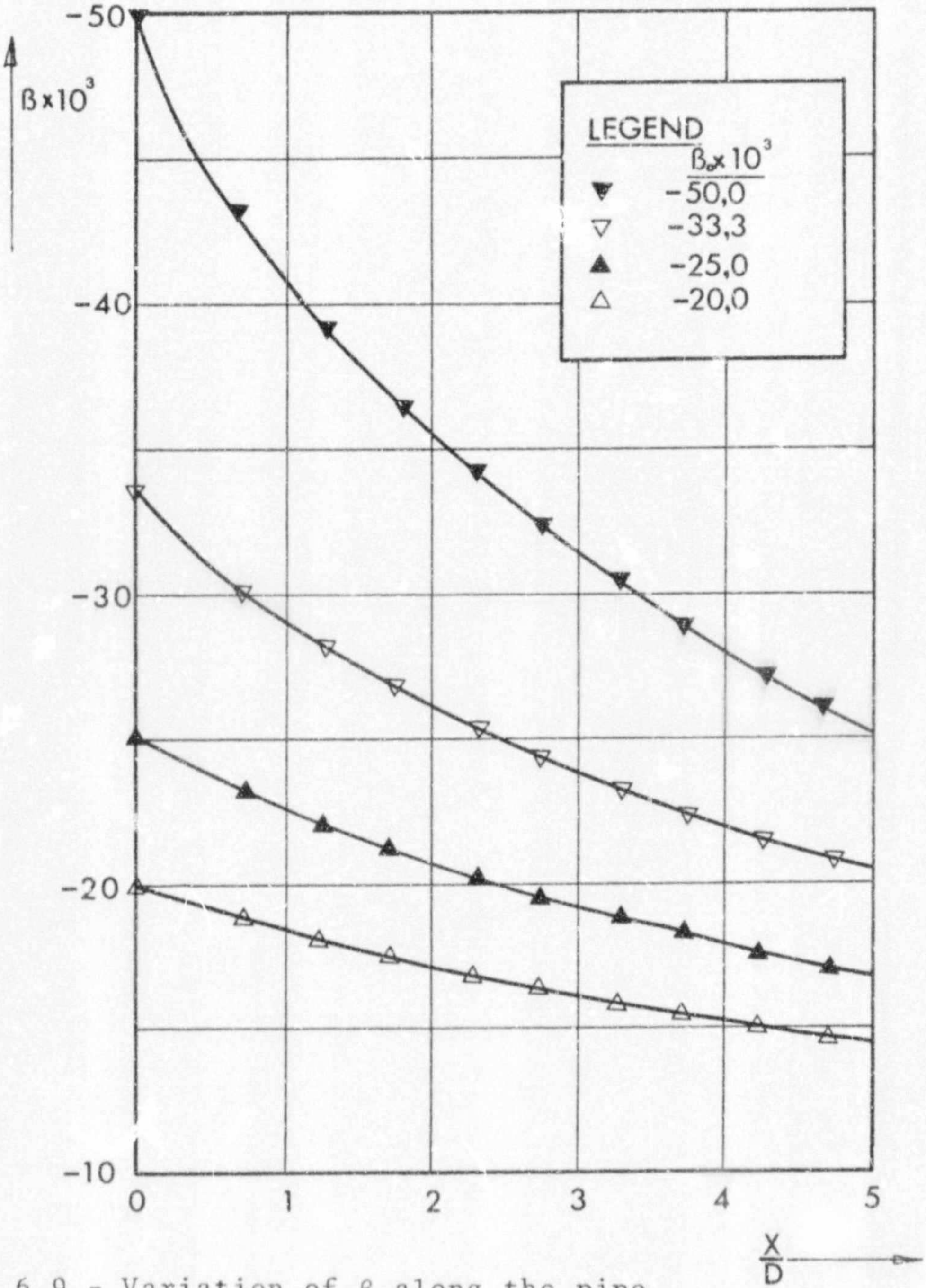

Fig 6.9 - Variation of β along the pipe for different initial blowing rates

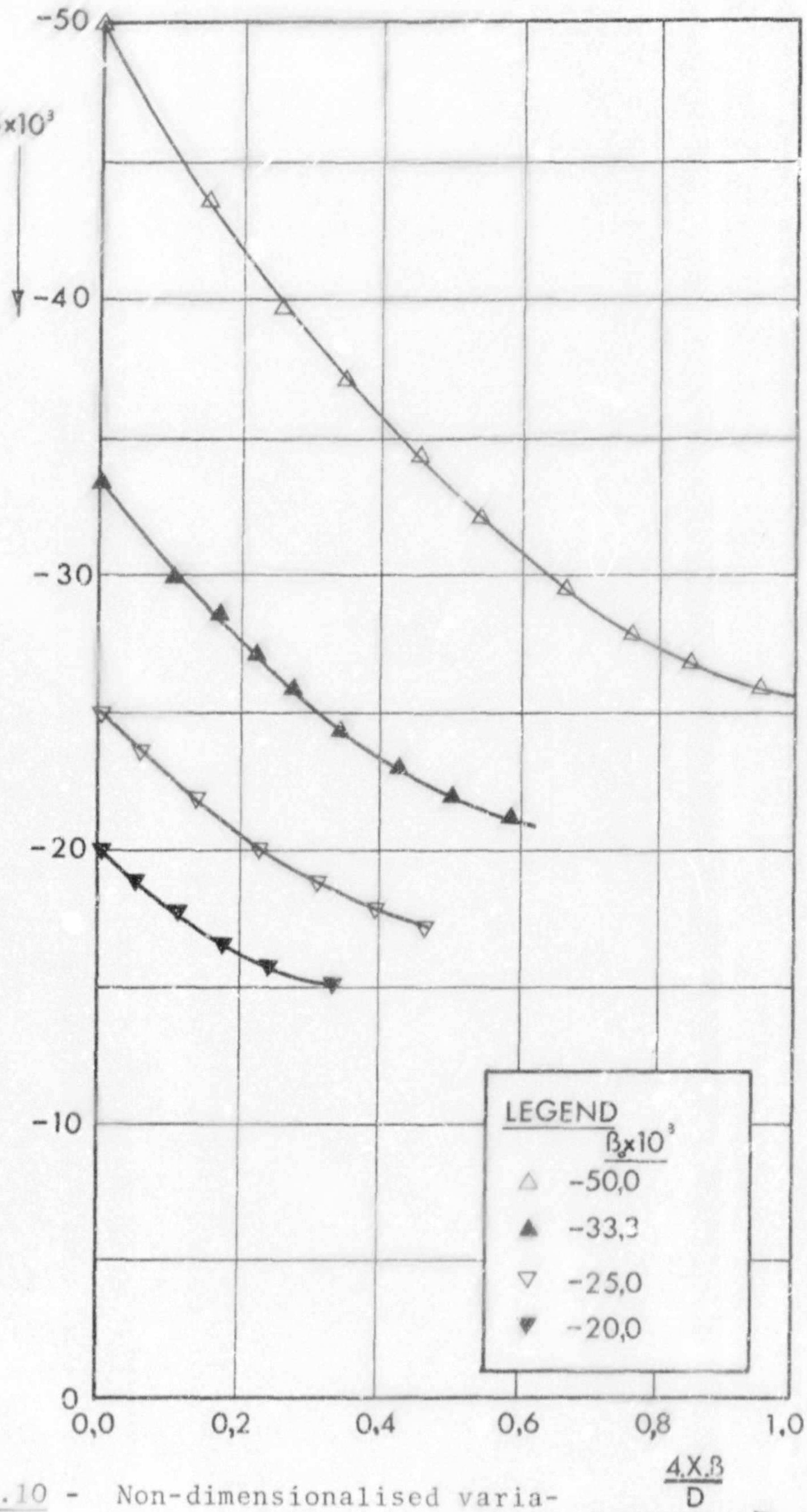

Fig 6.10 - Non-dimensionalised variation of β along the pipe for blowing

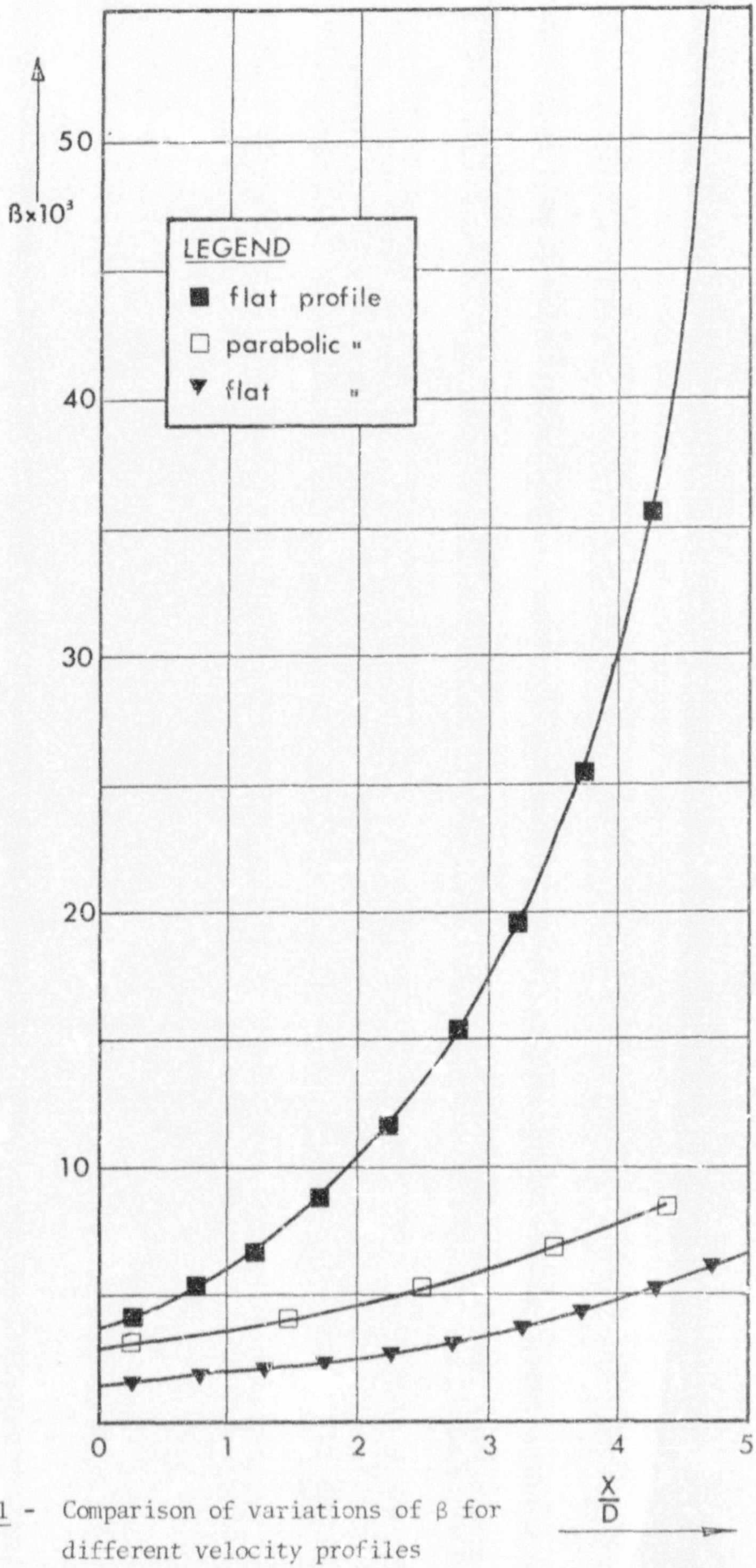

Fig 6.11 - Comparison of variations of β for different velocity profiles

Fig 6.12 - Visualisation of the flow field for:

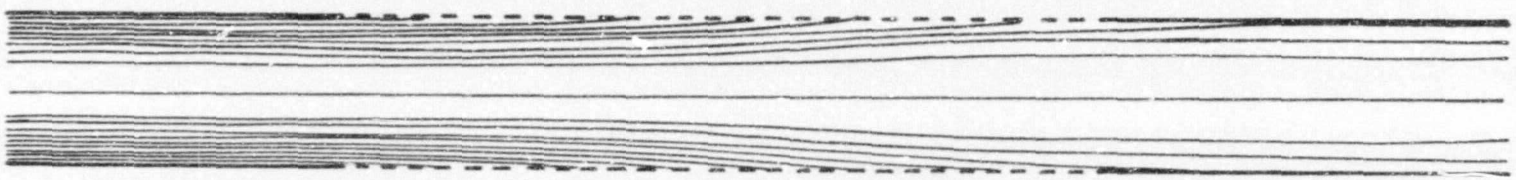

a) ratio of mass extracted to inflow = 0,66

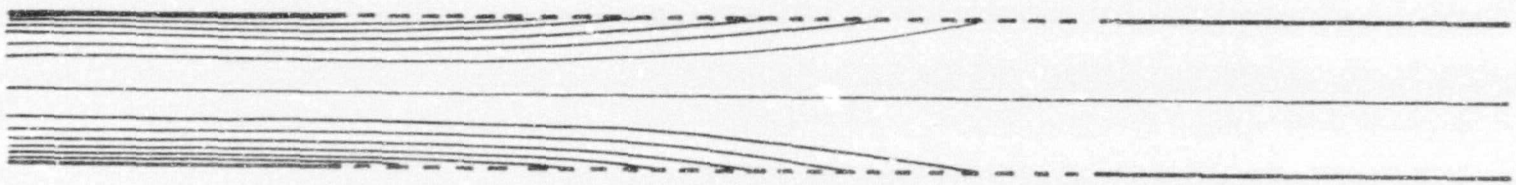

b) total mass extraction

Tests so far have only been discussed which have involved uniform suction or blowing along the length of the pipe. Figure 6.13, however, illustrates the effects of allowing the suction to vary according to the pressure difference across the pipe wall, as explained in section 3.9 and formulated in section 4.9. As fluid is removed through the wall so the velocity in the pipe decreases and hence the static pressure rises, forcing more fluid to pass through the wall, as shown by the increasing slope of the suction velocity graph with axial distance. It is expected that in practice the suction curves should be of this form although the slopes could be considerably less due to the pressure gradient across the wall being more noticeable than the axial one. This means that the pressure at the inlet to the pipe could be a lot higher than atmospheric pressure.

For various suction rates, and boundary conditions the radial velocity at a given axial location is plotted against radial position. The curves are shown in figure 6.14, they can be seen to be almost linear, decreasing from the suction velocity at the pipe wall to zero on the axis. The parabolic axial velocity does not have any effect on the shape of the curves. This is obviously due to the potential flow nature of the solution. The only curve that appears to be slightly different from the others is the one for the variable suction case. This tends to be slightly convex. The only possible explanation is that the radial velocity towards the axis of the pipe is influenced by the greater suction velocities further downstream and the radial velocities near the pipe wall are controlled directly by the suction velocity at the axial location under examination. This would tend to make the radial velocities towards the axis of the pipe greater than they would be for the constant suction case.